JGR Atmospheres

RESEARCH ARTICLE
10.1029/2022JD038228

Data- and Model-Based Urban O_3 Responses to NO_x Changes in China and the United States

Xiaokang Chen[1], Min Wang[1], Tai-Long He[2,3], Zhe Jiang[1], Yuqiang Zhang[4], Li Zhou[5], Jane Liu[6,7], Hong Liao[8], Helen Worden[9], Dylan Jones[2], Dongyang Chen[5], Qinwen Tan[10], and Yanan Shen[1]

[1]School of Earth and Space Sciences, University of Science and Technology of China, Hefei, China, [2]Department of Physics, University of Toronto, Toronto, ON, Canada, [3]Now at Department of Atmospheric Sciences, University of Washington, Seattle, WA, USA, [4]Big Data Research Center for Ecology and Environment, Shandong University, Qingdao, China, [5]College of Architecture and Environment, Sichuan University, Chengdu, China, [6]School of Geographical Sciences, Fujian Normal University, Fuzhou, China, [7]Department of Geography and Planning, University of Toronto, Toronto, ON, Canada, [8]School of Environmental Science and Engineering, Nanjing University of Information Science and Technology, Nanjing, China, [9]Atmospheric Chemistry Observations and Modeling Laboratory, National Center for Atmospheric Research, Boulder, CO, USA, [10]Chengdu Academy of Environmental Sciences, Chengdu, China

Xiaokang Chen and Min Wang authors contributed equally to this work.

Key Points:

- Data-based methods suggest VOC-limited regimes over northern inland China and transitional regimes over eastern United States urban areas
- GEOS-Chem simulation suggests strong NO_x-limited regimes
- Data-based methods have the potential to provide new insights for air quality regulations as a supplement to Chemical transport models

Supporting Information:

Supporting Information may be found in the online version of this article.

Correspondence to:

Z. Jiang and L. Zhou,
zhejiang@ustc.edu.cn;
lizhou@scu.edu.cn

Citation:

Chen, X., Wang, M., He, T.-L., Jiang, Z., Zhang, Y., Zhou, L., et al. (2023). Data- and model-based urban O_3 responses to NO_x changes in China and the United States. *Journal of Geophysical Research: Atmospheres*, *128*, e2022JD038228. https://doi.org/10.1029/2022JD038228

Received 21 NOV 2022
Accepted 5 OCT 2023

Abstract Urban air pollution continues to pose a significant health threat, despite regulations to control emissions. Here we present a comparative analysis of urban ozone (O_3) responses to nitrogen oxide (NO_x) changes in China and the United States (US) over 2015–2020 by integrating various data- and model-based methods. The data-based deep learning (DL) model exhibited good performance in simulating urban air quality: the correlation coefficients (R) of O_3 daily variabilities with respect to independent O_3 observations are 0.88 and 0.79 over N. China, 0.87 and 0.90 over S. China, and 0.87 and 0.49 over E. United States by the DL and GEOS-Chem chemical transport models, respectively. Furthermore, the data-based methods suggest volatile organic compound (VOC)-limited regimes in urban areas over northern inland China and transitional regimes over eastern US urban areas; in contrast, GEOS-Chem model suggests strong NO_x-limited regimes. Sensitivity analysis indicates that the inconsistent O_3 responses are partially caused by the inaccurate representation of O_3 precursor concentrations at the locations of urban air quality stations in the simulations, while the data-based methods are driven by the variabilities in local O_3 precursor concentrations and meteorological conditions. The O_3 responses to NO_x changes reported here provide a better understanding of urban O_3 pollution; for example, reductions in NO_x emissions are suggested to have resulted in an increase in surface O_3 by approximately 7 ppb in the Sichuan Basin in 2014–2020.

Plain Language Summary Ozone (O_3) at the surface level is an important pollutant with complicated photochemistry. Here we analyze the responses of urban O_3 concentrations to nitrogen oxide (NO_x) changes in China and the United States (US) over 2015–2020. The data-based methods suggest that NO_x emission declines have resulted in increases in urban O_3 concentrations over northern inland China, while urban O_3 concentrations over eastern US are less sensitive to NO_x changes. In contrast, GEOS-Chem simulation suggests that NO_x emission declines can result in dramatic decreases in urban O_3 concentrations over both China and the US. The derived O_3 responses in this work are helpful for making effective regulatory policies to control urban O_3 pollution.

1. Introduction

Chemical transport models (CTMs) have been widely used to interpret observed changing air quality and assess the efficacy of air quality regulations (Coggon et al., 2021; K. Li et al., 2021; Lu et al., 2021). However, despite advances in CTMs, it is still challenging to accurately simulate urban air quality due to uncertainties in physical and chemical processes (J. Chen et al., 2022; K. Li et al., 2019b), emission inventories (Jiang et al., 2022; Zheng et al., 2017) and coarse model resolutions (Benavides et al., 2021; Schaap et al., 2015). These model limitations have particularly large negative impacts on simulations of urban air quality in countries with high urbanization. For example, significant reductions in NO_x emissions (Jiang et al., 2022) are supposed to have led to the mitigation of O_3 pollution in inland China in recent years (X. Chen et al., 2021; K. Li et al., 2019a; Y. Liu & Wang, 2020; Z. Liu et al., 2021), but the prediction conflicts with the observed urban O_3 increase.

Recent advances in data-driven artificial intelligence techniques provide a new way to investigate air quality changes. For example, Zhong et al. (2021) constructed hourly gridded networks of fine particulate matter ($PM_{2.5}$) in China; T.-L. He et al. (2022) showed the capability of a deep learning (DL) model to predict surface O_3 in North America; and Han et al. (2022) exhibited good skill of a DL model to predict surface carbon monoxide (CO) in China. However, while artificial intelligence methods demonstrate good prediction capacity, their capability to explain the mechanism of observed air quality changes is uncertain. Can artificial intelligence methods provide new insights for air quality regulations as a supplement to CTM-based analysis to provide additional guidance for effective regulatory policies to control urban air pollution?

Similar to China, effective emission regulations have been employed to control tropospheric NO_2 and O_3 concentrations in the United States (US) (Chang et al., 2017; Jiang et al., 2022; Miyazaki et al., 2017). In this study, we developed a hybrid DL model based on convolutional neural networks (CNNs) and long short-term memory (LSTM) neural networks to evaluate urban O_3 responses to NO_x changes in China and the US over 2015–2020. The O_3 responses predicted by the DL model are further compared with the data-based lognormal fit approach (X. Chen et al., 2021) and a photochemical box model (X. Liu et al., 2019; Xue et al., 2013, 2016), as well as GEOS-Chem CTM with $0.5° \times 0.625°$ horizontal resolution. The comparative analysis by integrating various data- and model-based methods over two continents with different environmental, social, and economic developments can provide helpful information for making more effective regulatory policies to control urban air pollution globally.

2. Methodology and Data

2.1. MEE and AQS Surface NO_2 and O_3 Measurements

We use surface in situ hourly NO_2 and O_3 concentration data from the China Ministry of Ecology and Environment (MEE, https://quotsoft.net/air) and US Environmental Protection Agency Air Quality System (AQS, https://aqs.epa.gov/aqsweb/airdata/download_files.html#Raw) monitoring networks for the period 2015–2020. Concentrations were reported by the MEE in units of ug/m^3 under standard temperature (273 K) until 31 August 2018. This reference state was changed on 1 September 2018 to 298 K. We converted the O_3 and NO_2 concentrations to ppb and rescaled the postAugust 2018 concentrations to the standard temperature (273 K) to maintain consistency in the trend analysis. Following K. Li et al. (2020), O_3 and NO_2 observations over all stations, including those with partial records, are used in our analysis because of the limited influence on the derived O_3 trends (K. Li et al., 2020).

2.2. The Hybrid DL Model

As shown in Figure 1, the hybrid DL model is a combination of CNN and LSTM. The convolutional layers and max-pooling layers on the left side form the encoder for extracting features from the input data. The encoding process not only reduces the resolution of features but also compresses the high-resolution information into latent vectors that flow through the hidden layers. The decoder on the right side reconstructs the compressed latent features to high resolution through transposing convolution and upsampling layers. We add residual connections to the model, which can forward the high-resolution information to the decoder, contributing to the accuracy of model localization and speeding up the convergence of the training process. We use the squared error loss function. Since the model is a supervised architecture, the summertime maximum daily 8-hr average (MDA8) O_3 from the MEE and AQS monitoring networks are used as true values in the training process. The model obtains the predictions by forward propagation during each iteration and then iteratively updates the weights in the network using the backward propagation algorithm (LeCun et al., 1989; Rumelhart et al., 1986). In addition, we employ the adaptive gradient Adam optimizer, with high computational efficiency and low memory requirements, which can also accelerate the convergence of the cost function. Here are the major hyperparameters of the model: learning rate 0.0001; batch size 50; epochs 400; early stopping patience 20.

The input variables include nine meteorological variables ($0.5° \times 0.625°$ horizontal resolution) from Modern-Era Retrospective analysis for Research and Applications, Version 2 (MERRA-2): sea level pressure (SLP), surface incoming shortwave flux (SWGDN), surface temperature (TS), 2-m air temperature (T2M), 10-m eastward wind (U10M), 10-m northward wind (V10M), 2-m specific humidity (QV2M), total precipitation (PRECTOT) and total cloud area fraction (CLDTOT); and NO_2 concentrations from the MEE and AQS networks. The daily meteorological variables are obtained by averaging hourly data within 12:00–19:00 local time. The observed NO_2

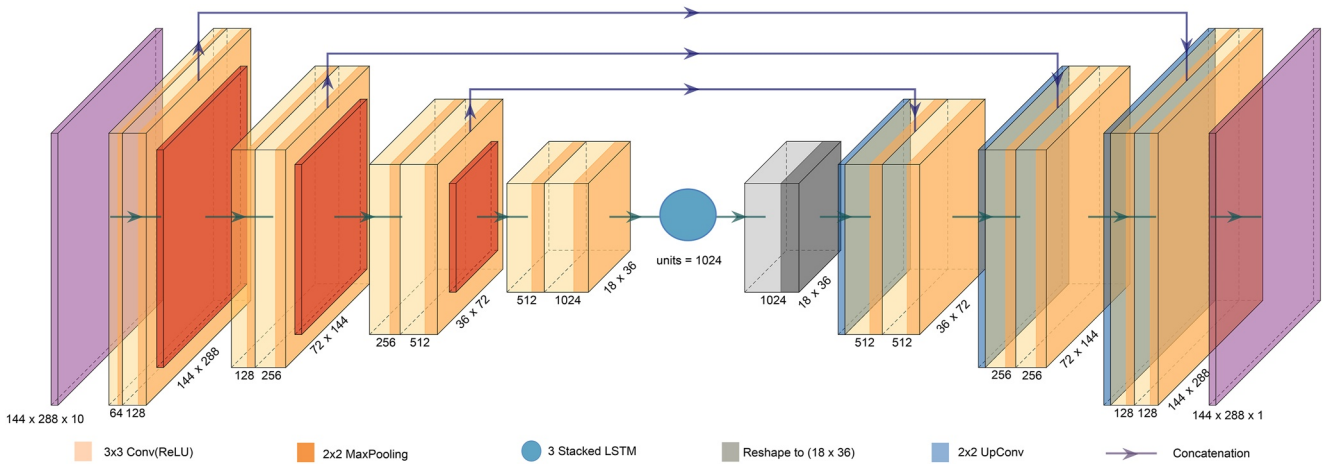

Figure 1. A hybrid deep learning model used in this paper. Nine meteorological variables and NO_2 observations from Ministry of Ecology and Environment and Air Quality System are used as input variables and the output is the MDA8 ozone. Both have 144 pixels in the latitudinal dimension and 288 pixels in the longitudinal dimension. The orange boxes represent 3 × 3 convolutional layers with ReLU as the activation function. The red boxes represent 2 × 2 max-pooling layers that can extract the most critical features. The blue circle represents 3 stacked long short-term memory cells, which take flattened latent vectors as input. The gray box is a reshaping layer. The light blue box is a transposed convolutional layer for upsampling the latent vectors. Light orange boxes after each transpose convolutional layer represent the features transferred from the encoder by the skip connections. The arrows on the top represent the direction of the skip connections.

and O_3 concentrations are interpolated into GEOS-Chem grids and processed as daily averages to match the spatial and temporal resolution of the input meteorological variables. The grids without air quality stations are defined as blank data in the model training. To enhance the efficiency and stability of neural network training, we normalize the input meteorological variables so that each variable has a similar range of values. The normalization is performed specifically by subtracting the mean from the original data and then dividing by the standard deviation so that the processed data are approximated to the standard normal distribution. The data from 2015 to 2018 are used as the training set to train the model, and the data from 2019 to 2020 are employed to evaluate the performance of the model as a test set.

2.3. GEOS-Chem Model Simulations

The GEOS-Chem CTM (http://www.geos-chem.org, version 12-8-1) is driven by assimilated meteorological data of MERRA-2 with nested 0.5° × 0.625° horizontal resolution. The GEOS-Chem model includes fully coupled O_3-NO_x-VOC-halogen-aerosol chemistry. The chemical boundary conditions are updated every 3 hr from a global simulation with 4° × 5° resolution. Emissions in GEOS-Chem are based on the Harvard-NASA Emission Component (HEMCO). Global default anthropogenic emissions are from the Community Emissions Data System (Hoesly et al., 2018). Regional emissions are replaced by Multiresolution Emission Inventory for China (MEIC) in China, MIX in other regions of Asia (M. Li et al., 2017) and NEI2011 in the US. The total anthropogenic NO_x and VOC emissions in the MEIC and NEI2011 inventories are further scaled to obtain the annual emissions in 2019 following X. Chen et al. (2021). Open fire emissions are from the Global Fire Emissions Database (van der Werf et al., 2010). Natural emissions of O_3 precursors, including NO_x from lightning and soil and VOCs from vegetation, are calculated on the basis of the assimilated MERRA-2 meteorology. The biogenic emissions of VOCs are calculated according to the Model of Emissions of Gases and Aerosols from Nature (MEGAN v2.1) (Guenther et al., 2006).

2.4. Photochemical Box Model

The photochemical box model (OBM) is configured with master chemical mechanisms (MCM v3.3.11, http://mcm.york.ac.uk/home.htt). The MCM-OBM model was designed to investigate the atmospheric oxidation processes of VOC species (X. Liu et al., 2019; Xue et al., 2013, 2016). The concentrations of sulfur dioxides (SO_2), CO, NO_x, and VOC, as well as meteorological parameters (atmospheric pressure, temperature, and relative humidity) from two monitoring sites in Chengdu city (in the Sichuan Basin [SCB]), were used as constraining parameters in the model. The MCM-OBM model simulations start at 12:00 local time for 8 hr, by inputting the

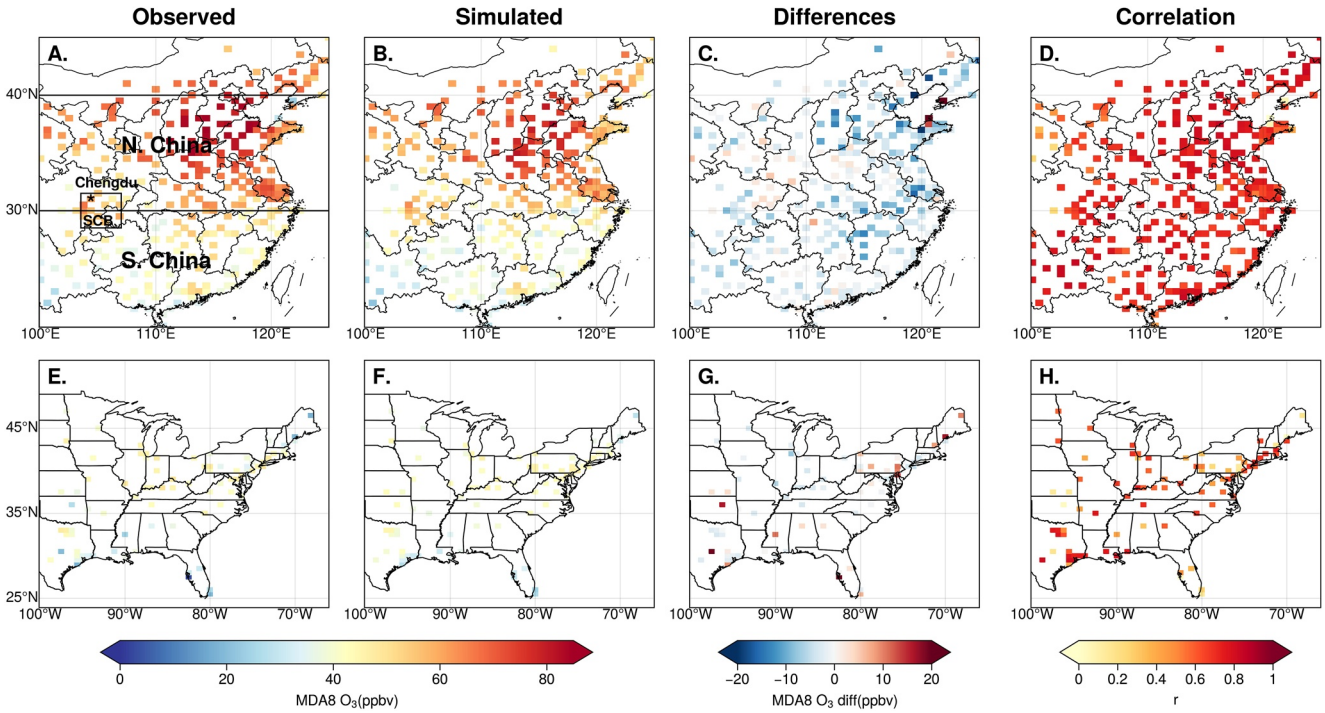

Figure 2. (a) Summertime MDA8 O_3 in 2019–2020 from the Ministry of Ecology and Environment urban stations. The station-based measurements are averaged and re-grided to 0.5° × 0.625° resolution. (b) Simulated O_3 concentrations by the deep learning (DL) model. (c, d) Differences and Pearson correlation coefficients between DL and observed O_3. (e–h) Same as panels (a–d), but for (e) United States by using Air Quality System O_3 observations. The black boxes in panel (a) define the domains for N. China, S. China, and the Sichuan Basin (SCB). The star in panel (a) represents the location of Chengdu City in the SCB.

observed O_3 concentration at the initial time. MCM-OBM simulations have been widely used to calculate the relative incremental reactivity to describe the response of O_3 to individual precursors (Z. He et al., 2019; J. Li et al., 2018; Tan et al., 2018; Wang et al., 2020).

3. Results

3.1. Surface O_3 Simulated by the DL Model

The hybrid DL model in this work is an autoencoder with the latent space represented by three LSTM cells (Figure 1). The input variables include nine meteorological variables as well as NO_2 concentrations from MEE and AQS monitoring networks. The optimization of the model is supervised by the "ground truth," which is the summertime MDA8 O_3 concentrations measured by the MEE and AQS networks. Only urban stations are considered in this work, and background stations are excluded. The DL model was trained to be a CTM-independent emulator with the NO_2-O_3 relationship observed by the MEE and AQS networks. Due to the lack of widely distributed long-term VOC observation data sets, VOC observations were not included in the model training by assuming limited changes in anthropogenic VOC emissions in the 6-year period because of their flatter trends with respect to changes in NO_x emissions (H. He et al., 2020; M. Li et al., 2019). We also assume limited influences from land usage changes on surface O_3 in the 6-year period. As the variabilities in biogenic VOC emissions are modulated by meteorological conditions such as temperature and solar radiation (Guenther et al., 2006), it is expected that our DL model, driven by meteorological variables, can predict the impact of biogenic VOC variabilities on surface O_3.

The observed surface MDA8 O_3 in the training period (2015–2018) exhibits higher O_3 in N. China and lower O_3 in S. China and E. US, which was well captured by our DL model (Figure S1 in Supporting Information S1). The DL model also captures the daily variabilities in summertime MDA8 O_3 concentrations over these three domains during the training period, with a Pearson correlation coefficient (R) larger than 0.95 (Figure S2 in Supporting Information S1). Furthermore, we successfully simulated the summertime MDA8 O_3 in the test period (2019–2020) using the DL model (Figure 2), with correlation coefficients slightly lower than those in the

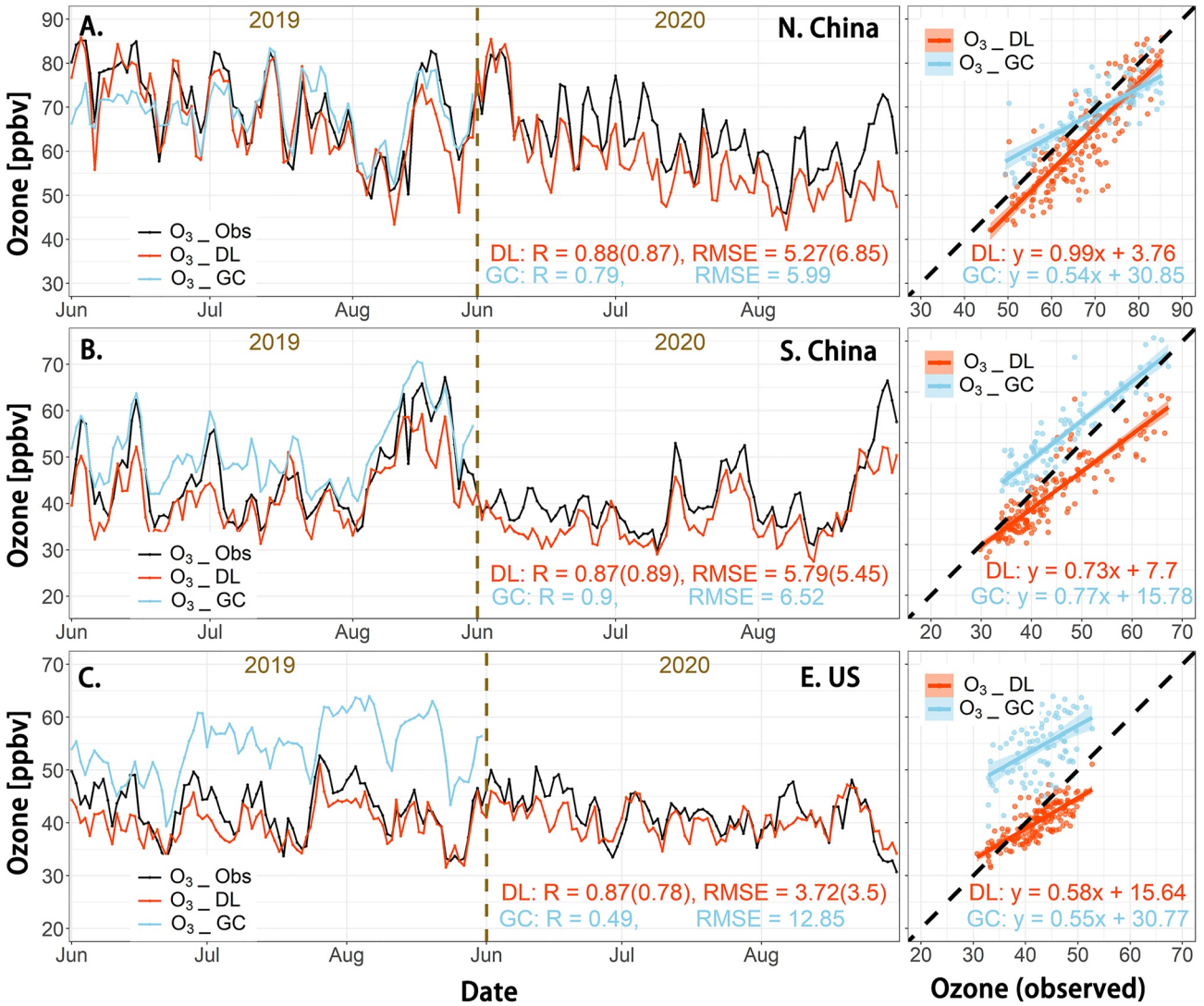

Figure 3. Daily variabilities of MDA8 O_3 from observations and simulations. (a, b) N. China and S. China (Ministry of Ecology and Environment, deep learning [DL], and GEOS-Chem) (c) E. United States (Air Quality System, DL, and GEOS-Chem). The domain definitions are shown in Figure 2. The numbers (and numbers in parentheses) of R and root mean square error (RMSE) represent correlation coefficient and RMSE for 2019, and 2019–2020, respectively.

training period (Figure S1 in Supporting Information S1). As shown in Figure 3, the DL-based daily O_3 concentrations (red lines) in 2019–2020 also exhibit good agreement with observations (black lines). The correlation coefficients between DL-based and observed O_3 in the test period are 0.87, 0.89, and 0.78 for N. China, S. China, and E. US, respectively.

Table S1 in Supporting Information S1 provides more information to evaluate the model performance. The normalized mean biases are 0.2%, 0.2%, and −5.2% in the training period, and −6.6%, −8.9%, and −4.8% in the test period for N. China, S. China, and E. US, respectively. The root mean square error are 2.14, 1.77, and 2.68 ppb in the training period, and 6.85, 5.45, and 3.50 ppb in the test period for N. China, S. China, and E. US, respectively. Furthermore, we find better model performance in China than in the E. US, for example, the slopes are 0.99, 0.73, and 0.58 in 2019–2020 for N. China, S. China, and E. US, respectively, which could be associated with the smaller number of observation stations in the US. It should be noted that our DL model validation replies to 20% (US) and 10% (China) O_3 observations in 2015–2018. Surface O_3 observations in 2019–2020 are independent observations, which are untouched in the model training, and thus, we can expect consistent model performance outside the period of 2015–2020.

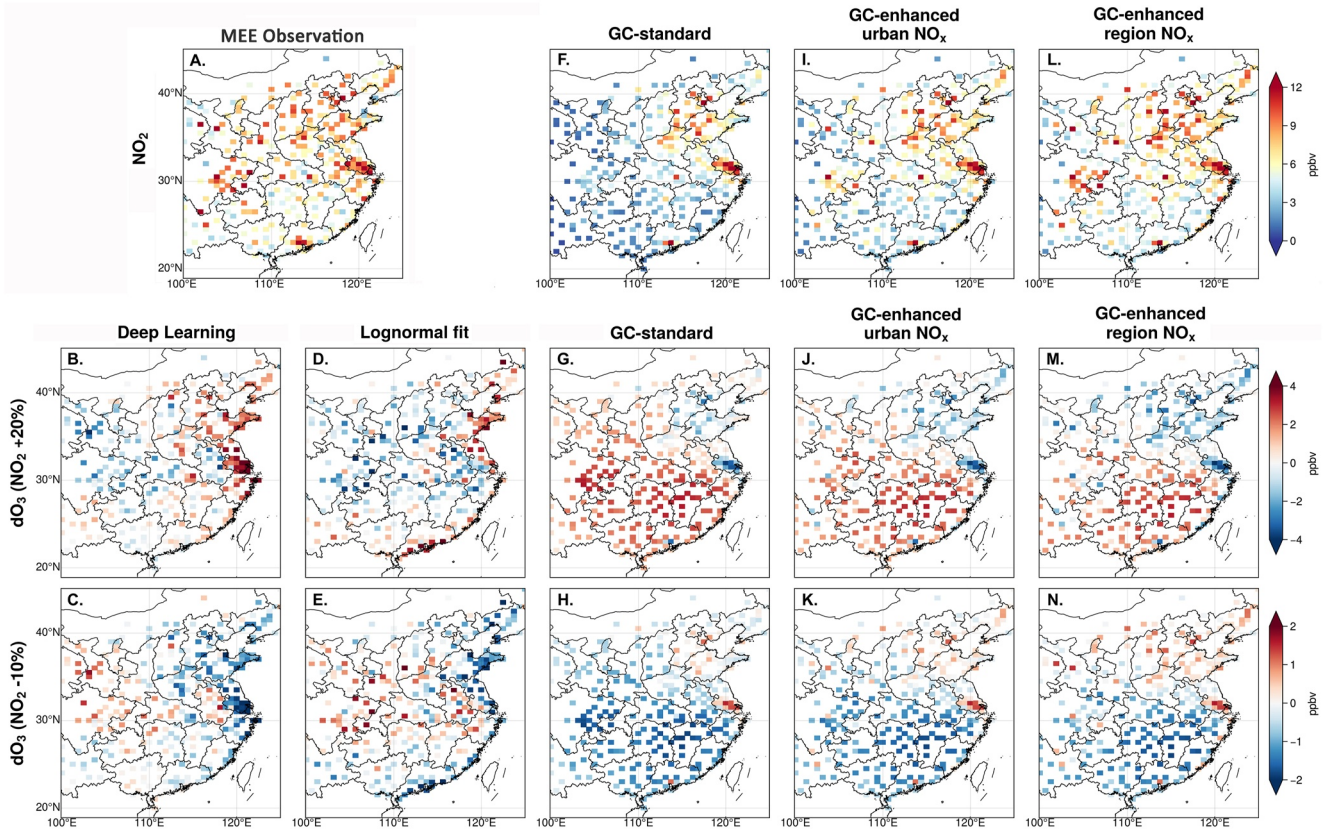

Figure 4. (a) Observed summertime surface NO_2 concentrations from the Ministry of Ecology and Environment (MEE) stations in 2019. The station-based measurements are averaged and re-grided to 0.5° × 0.625° resolution. The 8-hr range of surface NO_2 is selected according to the time range of MDA8 O_3. (b, c) Predicted responses of MDA8 O_3 in 2019 to NO_2 changes by the deep learning model. (d, e) Same as panels (b, c), but from analysis based on the lognormal fit. (f) Surface NO_2 concentrations from GEOS-Chem model standard simulation (Run 1), adjusted using the ratios of NO_y/NO_2 to consider the influences from reactive oxidized nitrogen compounds in the chemiluminescence analyzers. (g, h) Responses of MDA8 O_3 in 2019 to NO_x emission changes from GEOS-Chem model. (i–n) Similar to panels (f–h), but for sensitivity simulations by enhancing NO_x emissions over urban grids (Run 2) and urban + regional background (Run 3, see details in Supporting Information S1). The modeled NO_2 and O_3 are sampled at the locations and times of MEE surface measurements, and then averaged and re-grided to 0.5° × 625° resolution.

3.2. Consistent O_3 Responses in Data-Based Methods

Our DL model is driven by the inputted NO_2 concentrations and meteorological variables. We can thus predict the responses of surface O_3 to changes in NO_x emissions by adjusting the inputted NO_2 concentrations, as the responses of NO_2 concentrations to changes in NO_x emissions are broadly linear (Jiang et al., 2022). Figure 4a shows the summertime NO_2 concentrations from the MEE stations in 2019, with the same 8-hr periods as MDA8 O_3. Increasing the 2019 summertime NO_2 concentrations by 20%, the DL model predicts a widespread decrease in surface O_3 over N. China inland provinces (Figure 4b). The decreases in NO_2 concentrations before 2019 have thus led to increases in summertime surface O_3 over N. China inland provinces. The 2018–2020 Chinese Clean Air Action plan called for a 9% decrease in NO_x emissions (CSC, 2018), and thus, Figure 4c predicts surface O_3 changes driven by a 10% decrease in NO_2 concentrations. Continuous NO_x controls, as shown in Figure 4c, are predicted to result in the exacerbation of O_3 pollution over N. China inland provinces. Similarly, Figure 5a shows the summertime NO_2 concentrations from the AQS stations in 2019, which are much lower than NO_2 concentrations in China. The DL model predicts the widespread distribution of transitional regimes over E. US (i.e., slight red or blue shown in Figures 5b and 5c).

In a recent study, X. Chen et al. (2021) evaluated O_3 nonlinear chemistry regimes via lognormal fits of O_3 and NO_2 observations. Following X. Chen et al. (2021), Figure 6a shows the summertime O_3-NO_2 relationship over the SCB in 2014–2020. The data (dots) are regional averages of MDA8 O_3 and NO_2 concentrations, binned into 1 ppb NO_2 increments. Figure 6a indicates a VOC-limited regime over the SCB: reductions in NO_2 concentrations (*d*

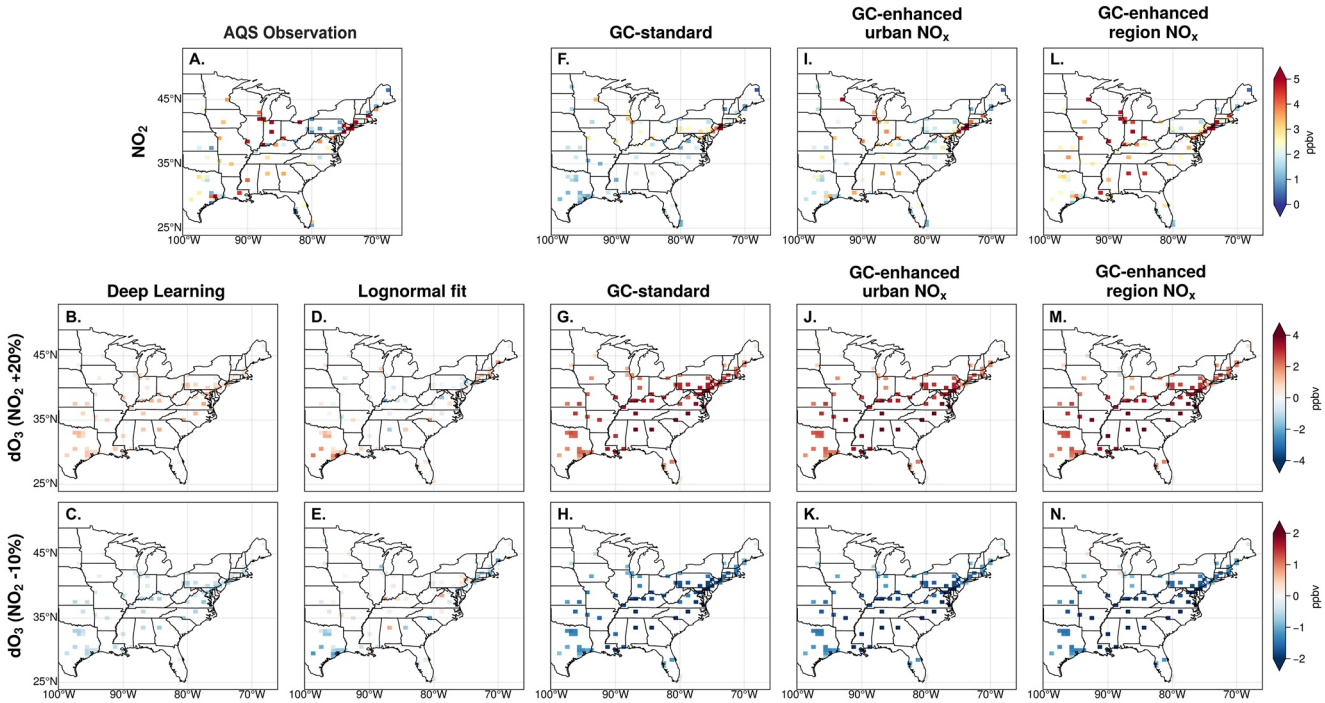

Figure 5. Same as Figure 4, but for E. United States by using Air Quality System observations.

NO_2) have led to an increase in surface O_3 ($d\,O_3$) in the SCB by approximately 7 ppb in 2014–2020 (based on the lognormal fitting line). This result is consistent with the observation-based OBM model with inputs of NO_x and VOC concentrations and meteorological parameters from observations: the OBM model indicates increases in O_3 with 60%–80% reductions in NO_x concentrations in Chengdu city (in the SCB) in 2017 and 2018 (Figure 6b). Following the approach shown in Figure 6a, lognormal fitting lines are produced for each 0.5° × 0.625° grid, which allows us to analyze O_3 nonlinear chemistry regimes in 2019. We find broadly good consistency between the DL-based prediction and the lognormal fit over China (Figures 4b and 4c vs. Figures 4d and 4e) and the US (Figures 5b and 5c vs. Figures 5d and 5e).

3.3. Surface NO_2 and O_3 Simulated by the GEOS-Chem Model

Figure 7 (blue lines) shows the daily variabilities in the modeled (GEOS-Chem) and observed NO_2 (based on the 8-hr periods as MDA8 O_3) in 2019 over China and the US. Here the modeled NO_2 are sampled at the locations and times of NO_2 observations and are adjusted using the ratios of NO_y/NO_2 to consider the influences from reactive oxidized nitrogen compounds in the chemiluminescence analyzers on the observed NO_2 concentrations (Lamsal et al., 2008; F. Liu et al., 2018), where $NO_y = NO_2 + \Sigma AN + 0.95 \times PAN + 0.35 \times HNO_3$ and ΣAN is the sum of all alkyl nitrate concentrations. We find dramatic underestimations in the modeled NO_2 concentrations: 5.2 and 7.8 ppb (N. China), 2.7 and 6.3 ppb (S. China), and 2.0 and 3.2 ppb (E. US) from GEOS-Chem simulations and observations from MEE and AQS stations, respectively. Figures 4f and 5f further show the distributions of summertime surface NO_2 concentrations from GEOS-Chem in 2019 over China and the US, respectively. The sampled NO_2 concentrations (Figure 4f) are comparable to the surface NO_2 observations (Figure 4a) over the NCP and Yangtze River Delta but lower in the rest of China. It seems that our model simulations (with 0.5° × 0.625° resolution) tend to underestimate urban NO_2 concentrations over areas with low regional population density.

Here we further investigate the consistency between modeled and observed daily variabilities of MDA8 O_3. As reported in recent studies (Guo et al., 2018; Kerr et al., 2019; McDonald et al., 2018), we find a significant overestimation of surface MDA8 O_3 (blue line in Figure 3c) with respect to the AQS O_3 observations over the US in 2019. The correlation coefficient between the modeled and observed MDA8 O_3 is as low as 0.49 over US in the CTM, which is much lower than the correlation coefficient in the DL model (0.87). However, we find comparable simulation capability of O_3 daily variabilities between GEOS-Chem and DL models in China: the correlation

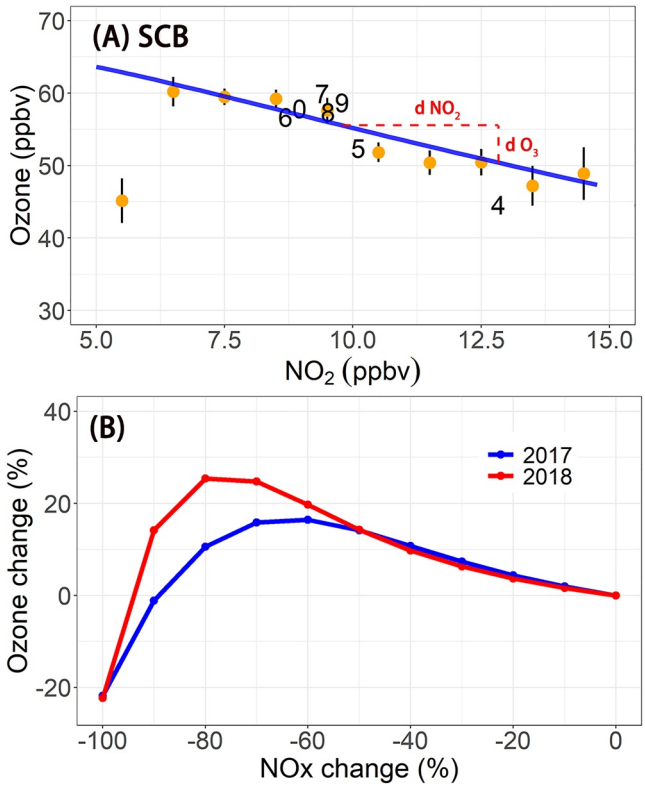

Figure 6. (a) Observed summertime O_3-NO_2 relationships from Ministry of Ecology and Environment stations with both O_3 and NO_2 measurements. The dots represent regional averages of MDA8 O_3 and NO_2 concentrations, binned into 1 ppb NO_2 increments. The 8-hr range of surface NO_2 measurements is selected according to the time range of MDA8 O_3. The blue line is lognormal fitting line. The error bars represent standard error. The numbers (0–9) represent the summertime mean O_3 and NO_2 abundances, and a number itself corresponds a year with the year's last digit during 2014–2020. (b) 8-hr averaged responses of O_3 to NO_x changes at the SL (103.93°N, 30.58°E, 20170801–20170815) and JPJ (104.05°N, 30.66°E, 20180601–20180610) sites in Chengdu, Sichuan Province. The simulations are performed using an OBM model with inputs of SO_2, CO, NO_x, and VOC concentrations and meteorological parameters from observations. Positive responses represent increases in O_3 within 8 hr (12:00–19:00 local time) due to a decrease in NO_x, indicating a VOC-limited regime.

coefficients between the modeled and observed MDA8 O_3 are 0.79 and 0.88 (N. China) and 0.90 and 0.87 (S. China) by GEOS-Chem and DL, respectively. As shown in Figure S3a in Supporting Information S1, the modeled regional background O_3 are comparable with urban O_3 observations in China; the modeled regional background O_3 is higher than the urban O_3 observations in the US (Figure S3b in Supporting Information S1). It should be noted that GEOS-Chem simulations are only performed in 2019 in this work to avoid the complicated perturbations of the 2019 novel coronavirus (COVID-19) on NO_x and VOC emissions.

3.4. O_3 Responses Simulated by the GEOS-Chem Model

Can the underestimated urban NO_2 concentrations pose a potential barrier to simulating urban O_3 responses? Figures 4g and 4h and Figures 5g and 5h show the model-based responses of surface O_3 to perturbations in anthropogenic NO_x emissions. We find different responses of O_3 to NO_2 changes between data- and model-based methods over both continents: VOC-limited regimes (blue in Figures 4b and 4d) over N. China and weak NO_x-limited regimes (slight red in Figures 4b and 4d) over S. China in the data-based methods, in contrast to widespread distributions of strong NO_x-limited regimes in GEOS-Chem (red in Figure 4g); transitional regimes over the eastern US (slight red or blue shown in Figures 5b and 5d) in the data-based methods, in contrast to widespread distributions of strong NO_x-limited regimes in GEOS-Chem (red in Figure 5g). Furthermore, as shown in Figure S4 in Supporting Information S1, the correlations in the grid-based O_3 responses between the DL and lognormal fit methods over E. China are 0.47 (Figure S4a in Supporting Information S1, NO_2 concentration decrease by 10%) and 0.42 (Figure S4b in Supporting Information S1, NO_2 concentration increase by 20%), in contrast to −0.43 and −0.45 between DL and GEOS-Chem simulations.

GEOS-Chem sensitivity simulations (Run 2, Table 1) adjust anthropogenic and soil NO_x emissions over urban grids (i.e., grids have MEE or AQS urban stations) using the ratios of observed/modeled NO_2. The adjustment of NO_x emissions over urban grids led to enhancements of sampled NO_2 concentrations in Figures 4i and 5i; however, they are still noticeably lower than observations (Figures 4a and 5a, also shown in Figure 7). Consequently, we further adjust regional background NO_x emissions based on the ratios of averaged observed/modeled NO_2 within neighboring grids (Run 3). As shown in Figures 4l and 5l (also shown in Figure 7), the sampled NO_2 concentrations in Run 3 match better with the observed urban NO_2 concentrations. It should be noted that the adjustments of NO_x emissions are designed to cover the underestimated urban NO_2 concentrations, which cannot be explained as an underestimation of NO_x emissions: it is unlikely that NO_x emissions in the emission inventory should be enhanced by 400% to match observations as shown in Figure S5 in Supporting Information S1.

The consistent NO_2 concentrations between the observations and sensitivity simulations lead to improvements in the modeled urban O_3 responses in China. For example, (Figure S6 in Supporting Information S1), the DL- and lognormal fit-based analyses predict -0.8 ± 0.8 ppb (Figure 4b) and -1.5 ± 1.5 ppb (Figure 4d) decreases in surface O_3 in the SCB in 2019, respectively, due to a 20% increase in anthropogenic NO_x emissions; in contrast, the modeled responses are increases in surface O_3 by 2.8 ± 0.2 ppb (Figure 4g), 1.2 ± 1.1 ppb (Figure 4j) and a decrease of -0.2 ± 1.2 ppb (Figure 4m). However, the enhanced NO_2 concentrations have a weaker influence on the modeled urban O_3 evolution in the US (Figure 5), and the model-based O_3 chemical regimes still show a large discrepancy with the reported transitional or VOC-limited regimes in recent studies (H. He et al., 2020; Jin et al., 2020). In a recent study, Zhu et al. (2023) suggests larger relative contributions of regional background O_3 to urban surface O_3 observations in the US than in China, which could be associated with the weaker influence of scaling NO_x emissions.

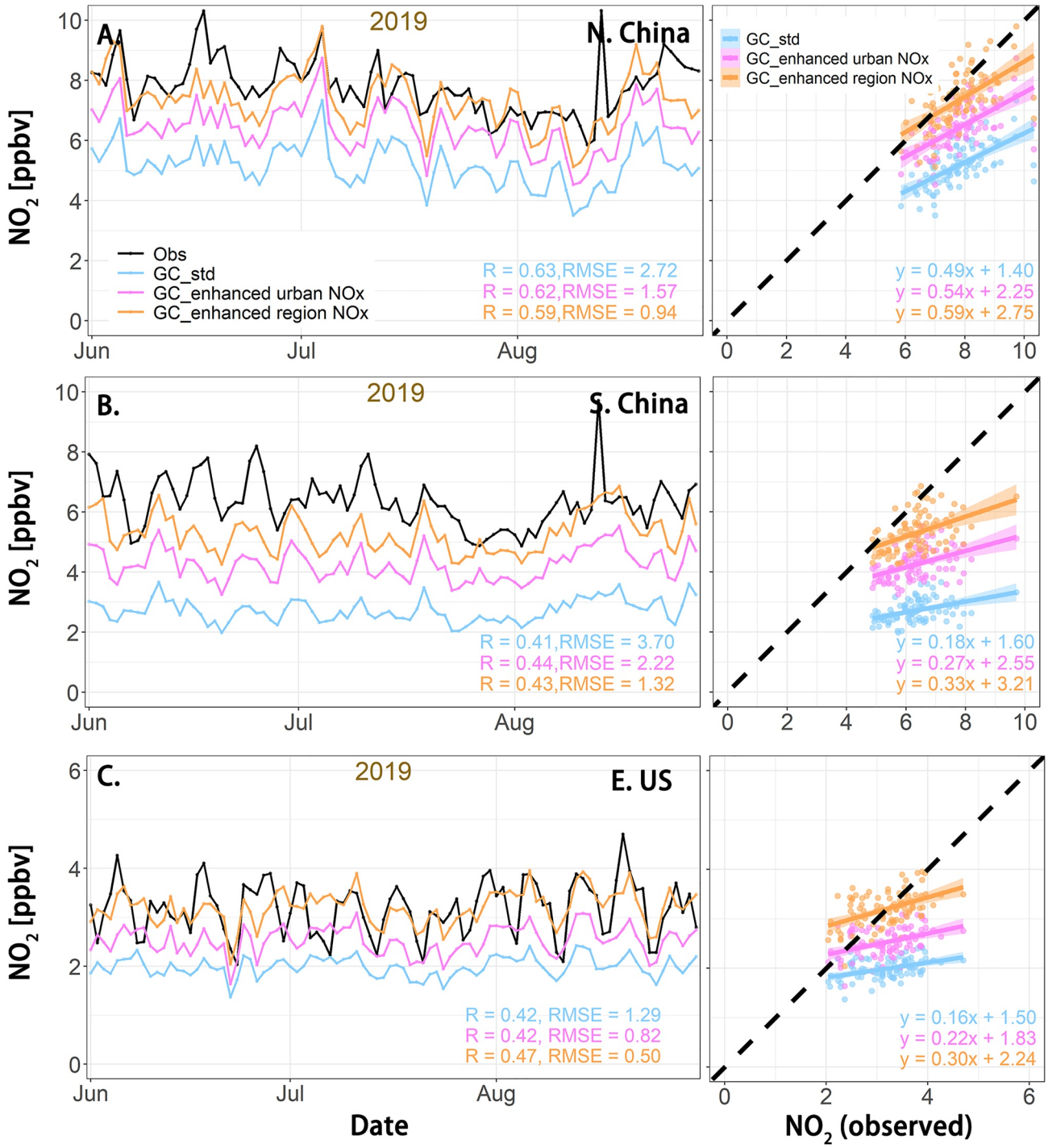

Figure 7. Daily variabilities of NO_2 (based on the 8-hr periods as MDA8 O_3) from observations and simulations. (a, b) N. China and S. China (Ministry of Ecology and Environment and GEOS-Chem) (C) E. United States (Air Quality System and GEOS-Chem).

3.5. Possible Sources of the Inconsistency in the Derived O_3 Responses

Both DL and photochemical box models require the input of atmospheric composition concentrations (NO_2 in the DL; NO_x and VOC in the photochemical box model) and meteorological variables at the local scale (i.e., at the location of in situ observation stations). Instead of calculating the detailed VOC-related chemical processes, the DL model simulates the impact of NO_2 on O_3 concentrations by assuming the mean states of

Table 1
GEOS-Chem Standard (Run 1) and Sensitivity (Runs 2–3) Simulations With 0.5° × 0.625° Horizontal Resolution in June–August 2019

GEOS-Chem simulations			
		Enhanced anthro + soil NO_x (A1)	anthro + soil NO_x factors (A2)
Run 1 (Standard)	#1(Base)	N/A	1.0
	#2		1.2
	#3		0.9
Run 2	#1(Base)	Urban grids	1.0
	#2		1.2
	#3		0.9
Run 3	#1(Base)	Urban grids + regional backgrounds	1.0
	#2		1.2
	#3		0.9

Note. The scaling factors (A1) to enhance anthropogenic and soil NO_x emissions over urban grids (i.e., grids have urban stations) and urban grids + regional background, based on the ratios between observed and modeled NO_2 concentrations, are shown in Figure S5 in Supporting Information S1. NO_x emissions over the highly industrialized NCP, YRD, and PRD are not adjusted.

anthropogenic VOC emissions in 2015–2020. The lognormal fit approach is a simplified version of the DL model that further assumes the mean states of meteorological variables in 2015–2020. Consequently, the three data-based methods have consistent mechanisms: they are all driven by atmospheric composition concentrations and meteorological variables at the local scale, despite more assumptions of mean states being considered in the DL and lognormal fit approaches. However, we may not expect the same accuracy between the DL and photochemical box models because of the assumption of mean states of anthropogenic VOC emissions.

We find noticeable differences between data-based methods and GEOS-Chem simulation. First, the horizontal resolution (0.5° × 0.625°) in our GEOS-Chem simulation could be too coarse to exactly simulate urban air quality at the local scale. For example, Benavides et al. (2021) compared the impacts of diesel NO_x emissions on urban NO_2 concentrations with both mesoscale (4 and 1 km resolutions) and street-scale models, and found a noticeable underestimation in the mesoscale model. Furthermore, regional transport plays a key role in GEOS-Chem simulations but does not affect data-based methods. For example, Figure S7a in Supporting Information S1 shows the impact of NO_x emission adjustment over urban grids (Run 2, Table 1) on regional background NO_2 concentrations, which leads to an increase in background NO_2 concentrations in the SCB by 2.05 ppb; Figure S7b in Supporting Information S1 further shows the impact of regional background NO_x emission adjustment (Run 3, Table 1) on urban NO_2 concentrations, which leads to an increase in urban NO_2 concentrations in the SCB by 2.56 ppb. In addition, uncertainties in physical, chemical processes and emission inventories (Jiang et al., 2022; K. Li et al., 2019b) could further affect the accuracy of model simulations. Consequently, the inconsistency in the derived O_3 responses may reflect the discrepancy in O_3 regimes at different spatial scales, that is, O_3 chemical regimes are VOC-limited at the local scale in urban centers; however, are NO_x-limited at larger regional scale when urban and rural O_3 regimes are mixed thorough grid average and regional transport. The lack of VOC observations in the DL model and uncertainties in physical, chemical processes and emission inventories in the simulations could also contribute to this inconsistency.

4. Conclusion

A comparative analysis by integrating various data- and model-based methods was presented in this work to investigate urban O_3 responses to NO_x changes in China and the US. Data-based methods, driven by atmospheric composition concentrations and meteorological variables at the local scale, suggest VOC-limited regimes in urban areas over northern inland China and transitional regimes over eastern US urban areas. In contrast, GEOS-Chem simulations suggest strong NO_x-limited regimes. This discrepancy could be partially caused by the inaccurate representation of O_3 precursor concentrations at the locations of urban air quality stations in the simulations

associated with the coarse model resolution (0.5° × 0.625°) which cannot match the exact locations of urban air quality stations and regional transport of atmospheric compositions which leads to the mixing of urban and rural O_3 regimes. The lack of VOC observations in the DL model and uncertainties in physical, chemical processes and emission inventories in the simulations could also contribute to this inconsistency.

The consistent NO_2 concentrations between the observations and sensitivity simulations lead to better agreement between data- and model-based methods, for example, the DL-based analysis predicts a -0.8 ± 0.8 ppb decrease in surface O_3 due to a 20% increase in anthropogenic NO_x emissions in the SCB in 2019 (Figure 4b); in contrast, the modeled responses are increases in surface O_3 by 2.8 ± 0.2 ppb (Figure 4g), 1.2 ± 1.1 ppb (Figure 4j), and a decrease of -0.2 ± 1.2 ppb in surface O_3 (Figure 4m) by gradually enhancing the modeled NO_2 concentrations. However, it should be noted that the adjustments of NO_x emissions in the sensitivity simulations are designed to cover the underestimated urban NO_2 concentrations, which cannot be explained as an underestimation of NO_x emissions.

The results illustrated in this work indicate the potential of data-based methods as a supplement to CTMs in providing new insights for air quality regulations. The derived O_3 responses to NO_x changes are helpful for a better understanding of urban O_3 pollution. It should be noted that the derived O_3 responses in this work are limited by the assumption of mean states of VOC in the DL- and lognormal fit-based analyses, although VOC observations were considered in our OBM model. More studies are suggested in the future to investigate the performance of data-based methods by including a few primary VOC species. We also advise more comparative analyses, particularly using CTMs with higher spatial resolutions, to investigate the advantages and disadvantages of data-based methods, which is critical for exploring better strategies for designing and using atmospheric observations.

Data Availability Statement

This analysis is supported by surface O_3 and NO_2 measurements provided by the China Ministry of Ecology and Environment (MEE, 2023) available at https://quotsoft.net/air/, US Environmental Protection Agency (AQS, 2023) available at https://aqs.epa.gov/aqsweb/airdata/download_files.html#Raw and a DL model (Jiang, 2022) available at https://doi.org/10.5281/zenodo.6017278.

Acknowledgments
The numerical calculations in this paper have been done on the supercomputing system in the Supercomputing Center of University of Science and Technology of China. *Funding sources*: This work was supported by the Hundred Talents Program of Chinese Academy of Science and National Natural Science Foundation of China (42277082 and 41721002).

References

AQS. (2023). Environmental Protection Agency: Surface O_3 and NO_2 measurements [Dataset]. Retrieved from https://aqs.epa.gov/aqsweb/airdata/download_files.html#Raw

Benavides, J., Guevara, M., Snyder, M. G., Rodríguez-Rey, D., Soret, A., Pérez García-Pando, C., & Jorba, O. (2021). On the impact of excess diesel NO_x emissions upon NO_2 pollution in a compact city. *Environmental Research Letters*, *16*(2), 024024. https://doi.org/10.1088/1748-9326/abd5dd

Chang, K. L., Petropavlovskikh, I., Cooper, O. R., Schultz, M. G., & Wang, T. (2017). Regional trend analysis of surface ozone observations from monitoring networks in eastern North America, Europe and East Asia. *Elementa: Science of the Anthropocene*, *5*, 50. https://doi.org/10.1525/elementa.243

Chen, J., Jiang, Z., Li, R., Liao, C., Miyazaki, K., & Jones, D. B. A. (2022). Large discrepancy between observed and modeled wintertime tropospheric NO_2 variabilities due to COVID-19 controls in China. *Environmental Research Letters*, *17*(3), 035007. https://doi.org/10.1088/1748-9326/ac4ec0

Chen, X., Jiang, Z., Shen, Y., Li, R., Fu, Y., Liu, J., et al. (2021). Chinese regulations are Working—Why is surface ozone over industrialized areas still high? Applying lessons from northeast US air quality evolution. *Geophysical Research Letters*, *48*(14), e2021GL092816. https://doi.org/10.1029/2021gl092816

Coggon, M. M., Gkatzelis, G. I., McDonald, B. C., Gilman, J. B., Schwantes, R. H., Abuhassan, N., et al. (2021). Volatile chemical product emissions enhance ozone and modulate urban chemistry. *Proceedings of the National Academy of Sciences of the United States of America*, *118*(32), e2026653118. https://doi.org/10.1073/pnas.2026653118

CSC. (2018). Chinese state council: Three-year action plan on defending the blue sky. Retrieved from http://www.gov.cn/zhengce/content/2018-07/03/content_5303158.htm

Guenther, A., Karl, T., Harley, P., Wiedinmyer, C., Palmer, P. I., & Geron, C. (2006). Estimates of global terrestrial isoprene emissions using MEGAN (model of emissions of gases and aerosols from nature). *Atmospheric Chemistry and Physics*, *6*(11), 3181–3210. https://doi.org/10.5194/acp-6-3181-2006

Guo, J. J., Fiore, A. M., Murray, L. T., Jaffe, D. A., Schnell, J. L., Moore, C. T., & Milly, G. P. (2018). Average versus high surface ozone levels over the continental USA: Model bias, background influences, and interannual variability. *Atmospheric Chemistry and Physics*, *18*(16), 12123–12140. https://doi.org/10.5194/acp-18-12123-2018

Han, W., He, T.-L., Tang, Z., Wang, M., Jones, D., & Jiang, Z. (2022). A comparative analysis for a deep learning model (hyDL-CO v1.0) and Kalman filter to predict CO concentrations in China. *Geoscientific Model Development*, *15*(10), 4225–4237. https://doi.org/10.5194/gmd-15-4225-2022

He, H., Liang, X.-Z., Sun, C., Tao, Z., & Tong, D. Q. (2020). The long-term trend and production sensitivity change in the US ozone pollution from observations and model simulations. *Atmospheric Chemistry and Physics*, *20*(5), 3191–3208. https://doi.org/10.5194/acp-20-3191-2020

He, T.-L., Jones, D. B. A., Miyazaki, K., Huang, B., Liu, Y., Jiang, Z., et al. (2022). Deep learning to evaluate US NO_x emissions using surface ozone predictions. *Journal of Geophysical Research: Atmospheres*, *127*(4), e2021JD035597. https://doi.org/10.1029/2021jd035597

He, Z., Wang, X., Ling, Z., Zhao, J., Guo, H., Shao, M., & Wang, Z. (2019). Contributions of different anthropogenic volatile organic compound sources to ozone formation at a receptor site in the Pearl River Delta region and its policy implications. *Atmospheric Chemistry and Physics*, *19*(13), 8801–8816. https://doi.org/10.5194/acp-19-8801-2019

Hoesly, R. M., Smith, S. J., Feng, L., Klimont, Z., Janssens-Maenhout, G., Pitkanen, T., et al. (2018). Historical (1750–2014) anthropogenic emissions of reactive gases and aerosols from the Community Emissions Data System (CEDS). *Geoscientific Model Development*, *11*(1), 369–408. https://doi.org/10.5194/gmd-11-369-2018

Jiang, Z. (2022). AI model for O_3 study in China [Software]. Zenodo. https://doi.org/10.5281/zenodo.6017278

Jiang, Z., Zhu, R., Miyazaki, K., McDonald, B. C., Klimont, Z., Zheng, B., et al. (2022). Decadal variabilities in tropospheric nitrogen oxides over United States, Europe, and China. *Journal of Geophysical Research: Atmospheres*, *127*(3), e2021JD035872. https://doi.org/10.1029/2021jd035872

Jin, X., Fiore, A., Boersma, K. F., Smedt, I., & Valin, L. (2020). Inferring changes in summertime surface ozone-NO_x-VOC chemistry over U.S. Urban areas from two decades of satellite and ground-based observations. *Environmental Science & Technology*, *54*(11), 6518–6529. https://doi.org/10.1021/acs.est.9b07785

Kerr, G. H., Waugh, D. W., Strode, S. A., Steenrod, S. D., Oman, L. D., & Strahan, S. E. (2019). Disentangling the drivers of the summertime ozone-temperature relationship over the United States. *Journal of Geophysical Research: Atmospheres*, *124*(19), 10503–10524. https://doi.org/10.1029/2019jd030572

Lamsal, L. N., Martin, R. V., van Donkelaar, A., Steinbacher, M., Celarier, E. A., Bucsela, E., et al. (2008). Ground-level nitrogen dioxide concentrations inferred from the satellite-borne Ozone Monitoring Instrument. *Journal of Geophysical Research*, *113*(D16), D16308. https://doi.org/10.1029/2007jd009235

LeCun, Y., Boser, B., Denker, J. S., Henderson, D., Howard, R. E., Hubbard, W., & Jackel, L. D. (1989). Backpropagation applied to hand written zip code recognition. *Neural Computation*, *1*(4), 541–551. https://doi.org/10.1162/neco.1989.1.4.541

Li, J., Zhai, C., Yu, J., Liu, R., Li, Y., Zeng, L., & Xie, S. (2018). Spatiotemporal variations of ambient volatile organic compounds and their sources in Chongqing, a mountainous megacity in China. *Science of the Total Environment*, *627*, 1442–1452. https://doi.org/10.1016/j.scitotenv.2018.02.010

Li, K., Jacob, D. J., Liao, H., Qiu, Y., Shen, L., Zhai, S., et al. (2021). Ozone pollution in the North China Plain spreading into the late-winter haze season. *Proceedings of the National Academy of Sciences of the United States of America*, *118*(10), e2015797118. https://doi.org/10.1073/pnas.2015797118

Li, K., Jacob, D. J., Liao, H., Shen, L., Zhang, Q., & Bates, K. H. (2019a). Anthropogenic drivers of 2013-2017 trends in summer surface ozone in China. *Proceedings of the National Academy of Sciences of the United States of America*, *116*(2), 422–427. https://doi.org/10.1073/pnas.1812168116

Li, K., Jacob, D. J., Liao, H., Zhu, J., Shah, V., Shen, L., et al. (2019b). A two-pollutant strategy for improving ozone and particulate air quality in China. *Nature Geoscience*, *12*(11), 906–910. https://doi.org/10.1038/s41561-019-0464-x

Li, K., Jacob, D. J., Shen, L., Lu, X., De Smedt, I., & Liao, H. (2020). Increases in surface ozone pollution in China from 2013 to 2019: Anthropogenic and meteorological influences. *Atmospheric Chemistry and Physics*, *20*(19), 11423–11433. https://doi.org/10.5194/acp-20-11423-2020

Li, M., Zhang, Q., Kurokawa, J. I., Woo, J. H., He, K., Lu, Z., et al. (2017). MIX: A mosaic Asian anthropogenic emission inventory under the international collaboration framework of the MICS-Asia and HTAP. *Atmospheric Chemistry and Physics*, *17*(2), 935–963. https://doi.org/10.5194/acp-17-935-2017

Li, M., Zhang, Q., Zheng, B., Tong, D., Lei, Y., Liu, F., et al. (2019). Persistent growth of anthropogenic non-methane volatile organic compound (NMVOC) emissions in China during 1990–2017: Drivers, speciation and ozone formation potential. *Atmospheric Chemistry and Physics*, *19*(13), 8897–8913. https://doi.org/10.5194/acp-19-8897-2019

Liu, F., Ronald, J. V., Eskes, H., Ding, J. Y., & Mijling, B. (2018). Evaluation of modeling NO_2 concentrations driven by satellite-derived and bottom-up emission inventories using in situ measurements over China. *Atmospheric Chemistry and Physics*, *18*(6), 4171–4186. https://doi.org/10.5194/acp-18-4171-2018

Liu, X., Lyu, X., Wang, Y., Jiang, F., & Guo, H. (2019). Intercomparison of O_3 formation and radical chemistry in the past decade at a suburban site in Hong Kong. *Atmospheric Chemistry and Physics*, *19*(7), 5127–5145. https://doi.org/10.5194/acp-19-5127-2019

Liu, Y., & Wang, T. (2020). Worsening urban ozone pollution in China from 2013 to 2017 – Part 2: The effects of emission changes and implications for multi-pollutant control. *Atmospheric Chemistry and Physics*, *20*(11), 6323–6337. https://doi.org/10.5194/acp-20-6323-2020

Liu, Z., Doherty, R. M., Wild, O., Hollaway, M., & O'Connor, F. M. (2021). Contrasting chemical environments in summertime for atmospheric ozone across major Chinese industrial regions: The effectiveness of emission control strategies. *Atmospheric Chemistry and Physics*, *21*(13), 10689–10706. https://doi.org/10.5194/acp-21-10689-2021

Lu, X., Ye, X., Zhou, M., Zhao, Y., Weng, H., Kong, H., et al. (2021). The underappreciated role of agricultural soil nitrogen oxide emissions in ozone pollution regulation in North China. *Nature Communications*, *12*(1), 5021. https://doi.org/10.1038/s41467-021-25147-9

McDonald, B. C., McKeen, S. A., Cui, Y. Y., Ahmadov, R., Kim, S. W., Frost, G. J., et al. (2018). Modeling ozone in the eastern U.S. using a fuel-based mobile source emissions inventory. *Environmental Science & Technology*, *52*(13), 7360–7370. https://doi.org/10.1021/acs.est.8b00778

MEE. (2023). China Ministry of Ecology and Environment: Surface O_3 and NO_2 measurements [Dataset]. Retrieved from https://quotsoft.net/air/

Miyazaki, K., Eskes, H., Sudo, K., Boersma, K. F., Bowman, K., & Kanaya, Y. (2017). Decadal changes in global surface NO_x emissions from multi-constituent satellite data assimilation. *Atmospheric Chemistry and Physics*, *17*(2), 807–837. https://doi.org/10.5194/acp-17-807-2017

Rumelhart, D. E., Hinton, G. E., & Williams, R. J. (1986). Learning representations by back-propagating errors. *Nature*, *323*(6088), 533–536. https://doi.org/10.1038/323533a0

Schaap, M., Cuvelier, C., Hendriks, C., Bessagnet, B., Baldasano, J., Colette, A., et al. (2015). Performance of European chemistry transport models as function of horizontal resolution. *Atmospheric Environment*, *112*, 90–105. https://doi.org/10.1016/j.atmosenv.2015.04.003

Tan, Z., Lu, K., Jiang, M., Su, R., Dong, H., Zeng, L., et al. (2018). Exploring ozone pollution in Chengdu, southwestern China: A case study from radical chemistry to O_3-VOC-NO_x sensitivity. *Science of the Total Environment*, *636*, 775–786. https://doi.org/10.1016/j.scitotenv.2018.04.286

van der Werf, G. R., Randerson, J. T., Giglio, L., Collatz, G. J., Mu, M., Kasibhatla, P. S., et al. (2010). Global fire emissions and the contribution of deforestation, savanna, forest, agricultural, and peat fires (1997–2009). *Atmospheric Chemistry and Physics*, *10*(23), 11707–11735. https://doi.org/10.5194/acp-10-11707-2010

Wang, M., Chen, W., Zhang, L., Qin, W., Zhang, Y., Zhang, X., & Xie, X. (2020). Ozone pollution characteristics and sensitivity analysis using an observation-based model in Nanjing, Yangtze River Delta Region of China. *Journal of Environmental Sciences*, *93*, 13–22. https://doi.org/10.1016/j.jes.2020.02.027

Xue, L. K., Gu, R., Wang, T., Wang, X., Saunders, S., Blake, D., et al. (2016). Oxidative capacity and radical chemistry in the polluted atmosphere of Hong Kong and pearl River Delta region: Analysis of a severe photochemical smog episode. *Atmospheric Chemistry and Physics*, *16*(15), 9891–9903. https://doi.org/10.5194/acp-16-9891-2016

Xue, L. K., Wang, T., Guo, H., Blake, D. R., Tang, J., Zhang, X. C., et al. (2013). Sources and photochemistry of volatile organic compounds in the remote atmosphere of western China: Results from the Mt. Waliguan observatory. *Atmospheric Chemistry and Physics*, *13*(17), 8551–8567. https://doi.org/10.5194/acp-13-8551-2013

Zheng, B., Zhang, Q., Tong, D., Chen, C., Hong, C., Li, M., et al. (2017). Resolution dependence of uncertainties in gridded emission inventories: A case study in Hebei, China. *Atmospheric Chemistry and Physics*, *17*(2), 921–933. https://doi.org/10.5194/acp-17-921-2017

Zhong, J., Zhang, X., Gui, K., Wang, Y., Che, H., Shen, X., et al. (2021). Robust prediction of hourly $PM_{2.5}$ from meteorological data using LightGBM. *National Science Review*, *8*(10), nwaa307. https://doi.org/10.1093/nsr/nwaa307

Zhu, R., Tang, Z., Chen, X., Liu, X., & Jiang, Z. (2023). Rapid O_3 assimilations – Part 2: Tropospheric O_3 changes accompanied by declining NO_x emissions in the USA and Europe in 2005–2020. *Atmospheric Chemistry and Physics*, *23*(17), 9745–9763. https://doi.org/10.5194/acp-23-9745-2023